Monthly Notices
of the
ROYAL ASTRONOMICAL SOCIETY

MNRAS **435,** 663–678 (2013) doi:10.1093/mnras/stt1324
Advance Access publication 2013 August 22

Study of young stellar objects and associated filamentary structures in the inner Galaxy

B. Bhavya,[1]⋆ Annapurni Subramaniam[2] and V. C. Kuriakose[1]

[1]*Department of Physics, Cochin University of Science & Technology, Kochi 682 022, India*
[2]*Indian Institute of Astrophysics, Bangalore 560034, India*

Accepted 2013 July 17. Received 2013 July 11; in original form 2013 February 27

ABSTRACT

Young stellar objects in the inner Galactic region $10^\circ < l < 15^\circ$ and $-1^\circ < b < 1^\circ$ were studied using GLIMPSE images and the GLIMPSE data catalogue. A total of 1107 Class I and 1566 Class II sources were identified in this Galactic region. With the help of GLIMPSE 5.8- and 8-μm images, we identified the presence of 10 major star forming sites in the Galactic mid-plane, 8 of which are filamentary while 2 are possible clusters of Class I and II sources. The length of the identified filaments are estimated as 8–33 arcmin (∼9–56 pc). The occurrence of a hub–filamentary system is observed in many filamentary star forming sites. Most of the Class I sources are found to be aligned along the length of these filamentary structures, while Class II sources have a random distribution. The mass and age distribution of 425 Class I and 241 Class II sources associated with filaments and clusters were studied through analysis of their spectral energy distribution. Most of the Class I sources detected have mass $>8\,M_\odot$, while Class II sources have relatively low masses. Class I sources have ages ≤ 0.5 Myr, while Class II sources have ages in the range ∼0.1–3 Myr. By combining our results with information from high mass star forming tracers, we demonstrate that large numbers of high-mass stars are being formed in the 10 regions studied here.

Key words: stars: formation – stars: low-mass – stars: massive – stars: pre-main-sequence – stars: protostars.

1 INTRODUCTION

It is important to understand star formation processes in the inner Galactic regions, as these environments have relatively high density and metallicity. Furthermore, they are regions where high-mass star formation occurs vigorously. It is interesting to note that the Galactic region $10^\circ < l < 15^\circ$ harbours many features such as filamentary structures, bubbles and H II regions that are observed only at longer wavelengths, indicating that this region is highly dynamic, active and young. Heavy obscuration of visible light prevents the study of the inner Galaxy using optical wavelengths. Owing to its high sensitivity and angular resolution, *Spitzer* (Werner et al. 2004) revolutionized our view of the inner Galaxy and enabled us to detect features that were not previously identified using optical wavelengths. The results are much more reliable and accurate than the previous poor-resolution far-infrared (far-IR) and millimetre observations. Mid-IR observations, which are less affected by dust extinction than the near-IR and optical wavelengths, obtained with the Infra Red Array Camera (IRAC) of *Spitzer* (Fazio, Hora & Allen 2004) lead to a deeper understanding of early star formation. The Galactic mid-plane, which contains the major sites of massive star formation, has been mapped with Science Legacy Program GLIMPSE surveys. The GLIMPSE I (Benjamin, Churchwell & Babler 2003) survey imaged the inner Galaxy from longitudes $l = 10^\circ$ to 65° and latitude $|b| \leq 1^\circ$ with resolution <2 arcsec in all IRAC bands.

Relative to the low-mass star formation processes, the high-mass star formation mechanism is poorly understood. Some of the reasons for the paucity of studies in this area are as follows: high-mass stars have a short pre-main sequence time-scale; most of the high-mass star forming regions are distant; it is difficult to observe the earliest stages of high-mass star forming processes; it is difficult to obtain a bona fide sample of high-mass stars; and the highly embedded nature of massive star forming sites makes it difficult to resolve and locate them. Hence, it has been difficult to characterize high-mass ($\geq 8\,M_\odot$) star forming processes. An understanding of high-mass protostars is essential in the study of the universal initial mass function, however. In this paper, we present a study of star forming regions at low Galactic latitudes. This region is suggested to be undergoing high-mass star formation, as revealed by previous studies. The region of interest is the inner Galactic plane, in the longitude–latitude range $10^\circ < l < 15^\circ$ and $-1^\circ < b < 1^\circ$, and close to the M17, W33 and W31 star forming regions. This region is located to the south-west of M17, which has many features that are not detectable in the optical but shows prominent features at longer wavelengths, including the mid-IR. The CO map in Sanders et al. (1986)

⋆ E-mail: bhavyab@cusat.ac.in

shows the presence of molecular clouds in this region. Several regions in this longitude–latitude range have been previously studied by others. Many of the studies are based on the H II region complexes such as W31 (G10.2-0.3 and G10.3-0.1) (Wilson 1974; Caswell et al. 1975; Corbel & Eikenberry 2004; Kim & Koo 2002; Furness et al. 2010; Beuther, Linz & Henning 2011) and W33 (Goss, Matthews & Winnberg 1978; Soifer et al. 1979; Stier et al. 1982; Goldsmith & Mao 1983; Haschisk & Paul 1983; Messineo et al. 2011) and also other ultra-compact H II regions, G10.6-0.4 (Sollins et al. 2005; Gerin et al. 2010; Neufeld et al. 2010; Klassen et al. 2011; Liu et al. 2011; Persson et al. 2012), G10.47+0.03 (Olmi, Cesaroni & Walmsley 1996; Pascucci et al. 2004; Rolffs et al. 2011), G10.62-0.38 (Beltran et al. 2011) etc. High-mass star formation in the IR dark cloud G11.11-0.12 (region 9 in our study), which is at a kinematic distance of 3.6 kpc (Clemens et al. 1986), has been studied using water and methanol masers by Pillai et al. (2006), using *Herschel* data by Henning et al. (2010) and more recently by Gomez et al. (2011). Although all the above regions are located in the first Galactic quadrant covering the near 3-kpc arm, the cited studies do not discuss their connection with the 3-kpc arm. According to Downes et al. (1980), the W31 complex is part of the 3-kpc arm, while Dame & Thaddeus (2008) find that the velocity peaks of W31 are not in accordance with the general 3-kpc arm kinematics. The detection of ultra-compact H II regions implies the primitive nature of this region. This might suggest that a large amount of molecular cloud in the inner galaxy is triggered to form stars, similar to 'global triggering', as suggested by Povich & Whitney (2010) in the case of M17SWex. This region is part of a number of surveys of methanol masers, IR dark clouds (IRDCs), starless clumps, H II regions etc and CO mapping. We have used the results from some of the previous surveys as tracers of high-mass star formation and to resolve the uncertainty in distance towards these regions.

Elongated structures of parsec scale seen in star forming complexes have been extensively studied by Myers (2009), who analysed the general properties of elongated structures observed in deep-optical, near-IR, CO mapping, IRAC and GLIMPSE/MIPSGAL images. In these images, the term 'hub' is used to describe a central blob of high column density, with a peak column density of 10^{22-23} cm^{-2}, and 'filament' denotes the associated feature of low column density. Smaller hubs tend to be relatively round, with fewer stars, lower column density and few radiating filaments. Larger hubs are more elongated, with more stars, higher column density, and 5–10 filaments. These filaments are nearly parallel to each other and are directed along the short axis of the hub with similar spacing and direction, forming a 'hub–filamentary system' (HFS). HFSs are seen in dust emission and absorption, and in molecular line emission. They are seen in optical dark clouds within a few hundred parsecs, and in IRDCs at distances of $\sim$3 kpc. In this region we notice filamentary features, with a few showing a HFS.

Here we make use of the point-source catalogue and image cutouts from the GLIMPSE I survey to demonstrate the young stellar content and features in the inner Galactic mid-plane. The YSO spectral energy distribution deviates at mid-IR wavelengths from normal photospheric emission. The *Spitzer*–IRAC sensitivity to mid-IR emission makes it the best tool with which to identify and characterize YSOs. Sources with excess mid-IR emission are classified as Class I (still embedded and accreting from dense spherical envelopes) or Class II (slightly more evolved pre-main sequence stars with circumstellar discs) (Lada et al. 2006; Gutermuth, Myers & Megeath 2008). The mass and the age range of YSOs in each region are estimated and used to elucidate the ongoing star formation and the filamentary structure.

This paper is structured as follows. Section 2 describes the archival data catalogues we used for the study of Galactic central regions. In Section 3 we detail the analysis and results, including classification of IRAC sources, identification of filamentary structures and clusters, spectral energy distribution fitting and parameter estimations, with a note on the distances and finally the description of each filaments and clusters. In Section 4 we include a brief discussion, and we summarize our main findings in Section 5.

2 ARCHIVAL DATA CATALOGUES USED FOR THIS STUDY

In order to understand the details of star formation in the region of interest, we combine the following archival data with the YSOs identified in this study. As these sources are tracers of high-mass star formation, they will be used to compare the masses and ages of the YSOs studied here. Because we do not have any distance estimate towards the YSOs studied here, we use the distance estimate for the sources in the archival data to obtain a possible range of distances to the YSOs. As some of the sources are noted in the literature to be associated with the inner spiral arms of the Galaxy, we use this information to connect the features identified in this study with the spiral structure of the inner Galaxy.

Infrared dark clouds (IRDCs)

IRDCs, which appear as silhouettes in the general Galactic mid-IR background, are the precursors of cluster-forming molecular clumps (Carey et al. 1998; Jackson et al. 2008), and IRDC cores host the very earliest phases of high-mass star formation (Rathborne et al. 2005; Rathborne, Jackson & Simon 2006; Simon et al. 2006; Rathborne, Simon & Jackson 2007). We have taken the catalogue from Peretto & Fuller (2009), which provides a complete sample of IRDCs in the Galactic range $10^\circ < |l| < 65^\circ$ and $|b| < 1^\circ$ using GLIMPSE and MIPSGAL surveys.

Methanol masers

According to Green et al. (2009), the methanol maser transition at 6.7 GHz has been observed towards early hot-core phases of star formation processes and has been found to be associated with tracers of high-mass star formation in IRDCs (Ellingsen 2006) and extended green objects (EGOs) (Cyganowski et al. 2008). Using the Methanol Multibeam (MMB) survey, Green et al. (2009) and Green et al. (2010) conducted a search for methanol masers and showed that significant star formation is occurring in the 3-kpc arm, which is found within 15° of the Galactic Centre. MMB detected more than 200 methanol masers in the region $15^\circ < l < -15^\circ$, and 49 of them have a velocity peak matching that of the near and far 3-kpc arms. Among them, 52 sources are located in our region of interest, of which four are identified as 3-kpc-arm signatures and two as far-arm features by Green et al. (2010).

Starless clumps

Using the ATLASGAL survey at 870 μm, Tackenberg et al. (2012) searched for dense gas condensations. Along with the GLIMPSE catalogue and 24-μm MIPSGAL images, this survey showed the existence of starless cores, which may form high-mass stars, in the Galactic region $10^\circ < l < 20^\circ$ and $|b| < 1^\circ$. The catalogue also provides distances (both far and near) towards these objects.

IR bubbles/H II regions

IR bubbles, some of the most spectacular objects in the GLIMPSE/MIPSGAL images, are the H II regions produced by radiation and wind from O and early B type stars of age $\sim 10^6$ yr

(Churchwell et al. 2009) and are therefore located at sites of recent massive star formation. Anderson et al. (2011) present the catalogue of H II regions in the Galactic region $343^\circ \leq l \leq 67^\circ$ and $|b| \leq 1^\circ$.

Radio sources

Galactic radio sources were taken from the radio continuum survey (CORNISH survey) by Purcell et al. (2013), targeting ultra-compact H II regions (UCHIIs) in high-mass star formation. The CORNISH project covers the northern GLIMPSE region ($10^\circ < l < 65^\circ$) using the Very Large Array at 5 GHz. We identified 10 such radio sources to be located in our longitude–latitude range.

We also show the locations of two high-mass protostellar objects (HMPOs) from Grave & Kumar (2009) and EGOs as tracers of massive young stellar objects (MYSOs) from Cyganowski et al. (2008) (four 'likely' MYSO ouflows and one 'possible' MYSO outflow) situated in our region of study. The spatial association of these sources (mainly as tracers of high-mass star formation) and YSOs identified in our analysis will be discussed in later sections.

3 ANALYSIS AND RESULTS

3.1 Classification of IRAC sources

More than 5 million sources from the GLIMPSE I survey in the longitude–latitude range $l = 10^\circ < l < -15^\circ$, $-1^\circ < b < 1^\circ$ were examined to identify candidate YSOs. As only *Spitzer*-IRAC magnitudes are used in the identification of YSOs, in order to improve the reliability we have taken only those IRAC sources with error less than 0.1 mag in all IRAC bands. The contamination from non-YSO sources and the effect of reddening need to be eliminated to create a bona fide sample of YSOs. We follow the Gutermuth et al. (2009, hereafter G09) procedure to remove background contamination and to select Class I and Class II sources. A brief outline of the five steps used to identify YSOs is given here.

G09 proposed an empirical scheme for identifying and classifying YSOs on the basis of mid-IR magnitudes and colours eliminating possible contaminants. According to Stern et al. (2005), galaxies dominated by polycyclic aromatic hydrocarbon (PAH) emission (normal star forming galaxies) show an excess in the 4.5- and 5.8-μm band passes, and broad-line active galactic nuclei (AGNs), having non-stellar spectral energy distributions, exhibit mid-IR colour indices similar to YSOs. Only very few (three) PAH emission sources and no AGN sources are identified in our sample when giving respective colour cuts based on G09.

The high-velocity outflows from protostars colliding with the surrounding molecular cloud cause unresolved blobs of shock emission and are sensitive to the 4.5-μm IRAC band, as it covers molecular hydrogen emission lines. By using G09 constraints in the [4.5]–[5.8] versus [3.6]–[4.5] colour space, we detect 19 sources as shock emission sources and remove them. Additional contaminants are spurious excess emission in the 5.8- and 8.0-μm band passes caused by PAH emission sources, which contaminate the photometric apertures of some faint field stars. There were 13 563 such contaminants.

After removing the above-mentioned contaminants, sources that satisfy the conditions of protostellar colours are classified as Class I sources. Fig. 1(a) shows the Class 1 sources (red triangles), other contaminants such as shock emission sources (blue) and PAH aperture contaminants (green) and the unclassified remaining sources (black). First, these Class I sources are extracted. Later, from the remaining sources, those with consistent colours of pre-main sequence stars having a circumstellar disc are classified as Class II sources. Fig. 1(b) shows Class II sources (red) and unclassified sources (black), which mostly consist of stars close to the main sequence. There are 1107 Class I sources and 1566 Class II sources identified in the region of interest. The GLIMPSE catalogue also provides 2MASS magnitudes for these sources. All these sources have 2MASS magnitudes, but only 103 Class I and 1090 Class II sources have 2MASS magnitudes with error less than 0.1 mag. We have not de-reddened IRAC colours. We caution that reddening can affect the the number of Class I and II sources identified. The extinction vectors (Flaherty et al. 2007) corresponding to $A_k = 5$ mag are shown in Fig. 1. As our study does not aim to obtain a complete census of YSOs in this region, but to understand the nature and location of early star formation, we do not attempt to achieve the completeness limit in detecting YSOs. Because an upper limit for the error in the IRAC magnitudes is set, our estimation of YSOs is a lower limit of the number of YSOs present in this location. Sources identified here are likely to be genuine detections and will help us to derive reliable properties of these sources as well as the star formation sites.

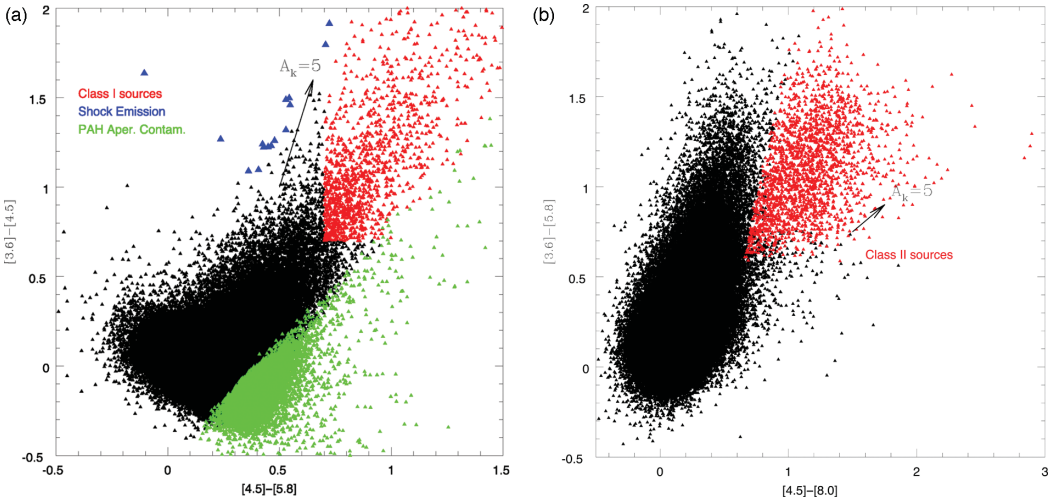

Figure 1. IRAC colour–colour diagrams showing YSOs and non-YSO sources. (a) Shock emission sources are represented by blue triangles, PAH aperture contaminants by green triangles, and Class I sources by red triangles. (b) Class II sources are represented by red triangles. Unclassified sources are represented by black triangles in both figures. An extinction vector corresponding to $A_k = 5$ mag is shown.

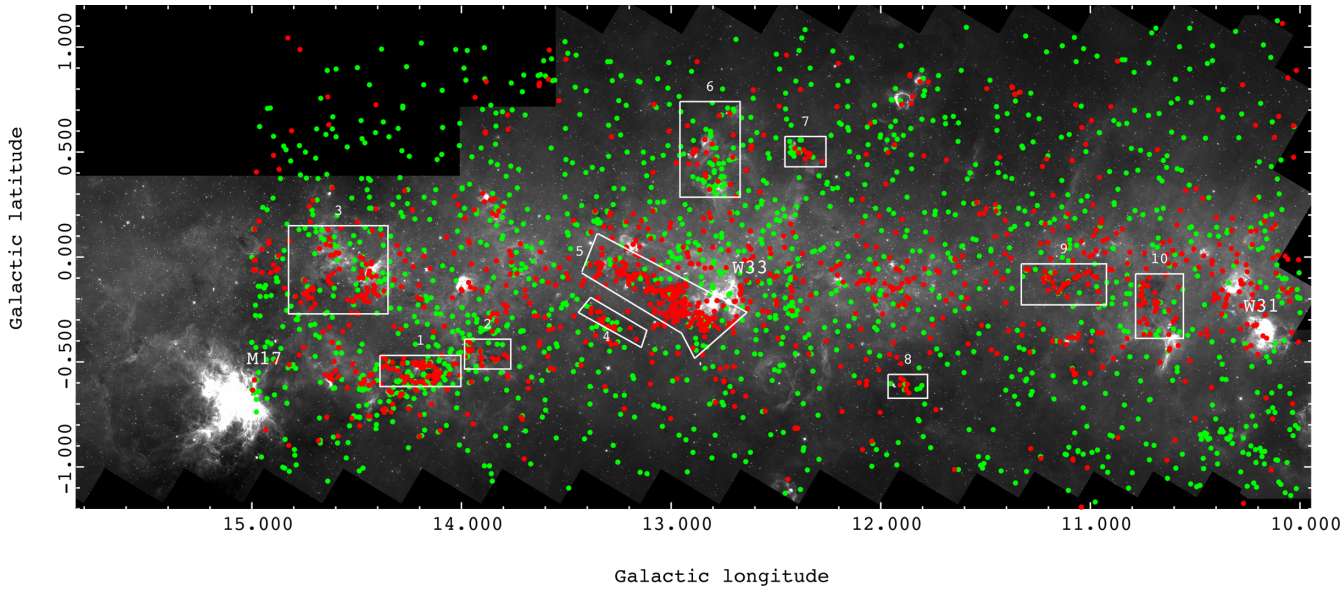

Figure 2. The region of our study as seen in the GLIMPSE 5.8-μm image. The *x*-axis is Galactic longitude, *l*, and the *y*-axis is Galactic latitude, *b*. The distributions of Class I sources (red points) and Class II sources (green points) in the region are shown. Regions marked inside the white boxes are the identified star formation sites. The locations of M17, W33 and W31 are also shown.

We point out the caveats and drawbacks of this study. Because only those sources with sufficient flux in all IRAC bands are considered in this study, faint low-mass Class I and II sources, evolved Class II sources and distantly located sources will be missed. The reduced number of these sources in our study is due to the sample selection and not to the absence of these sources in the region. There will also be source contamination from edge-on disc sources and reddened Class II sources, which mimic the colours of Class I sources. Gutermuth et al. (2009) give an upper limit for the edge-on disc source confusion as 3.3 ± 1.5 per cent. Kryukova et al. (2012) showed that there would be 4 per cent contamination owing to edge-on sources in their YSO sample. We assume a similar fraction of edge-on sources in our sample. The major impact of not using MIPSGAL data is that we are unable to identify reddened Class II sources.

In order to understand the distribution of these sources, the locations of Class I and Class II sources in the region studied are shown in Fig. 2. The locations of M17, W31 and W33 are also shown. It can be seen that the Class I sources are located in groups, whereas the Class II sources are located all over the region. The Class I sources are distributed very close to the Galactic plane, except in the M17SWex region. Specific locations of Class I groups can be identified and found to coincide with the locations of other tracers of high-mass star formation. The Class II sources do not show any preferential confinement to the Galactic plane. They are distributed randomly in the region, except for a couple of clusters. Thus, the Class I sources are likely to be associated with sites of high-mass star formation, most of which are located along the Galactic plane in the longitude–latitude range studied.

3.2 Filamentary structures and hub–filamentary systems

The 5.8- and 8-μm images from GLIMPSE reveal the presence of filamentary structures in the region, which appear as dark patches in mid- and far-IR images of the region. Close inspection of the images reveals several tiny filaments emanating from the main filament, forming a HFS. Class I sources are found to be aligned as a string along the length of these filamentary structures. We identify eight such filamentary structures of star forming regions and two candidate clusters of Class I and Class II sources in the entire region, each of which will be described in detail in Section 3.5. Filamentary structures are assumed to be primitive star forming sites, whereas the candidate clusters are slightly evolved. The locations of these identified regions are marked in Fig. 2. We have defined boxes to differentiate the filamentary regions and clusters from the background. Although the sizes of the boxes do not delimit the actual physical extent of each region, we have considered only those sources inside the boxes for further analysis. The sizes and shapes of the boxes that define the boundaries of the regions are defined to include most of the filamentary structure as seen in the images. We study the YSOs in these structures and correlate the locations of Class I and II YSOs with the filamentary structures to obtain the nature of the star formation they host. Although the Class II sources are randomly distributed in these regions (except for the regions near W33 and near M17SWex, where we can see a preferential clustering of Class II sources), Class I sources are either clumpy or closely associated with the filaments. In the entire region, we detect more Class II sources than Class I sources, with a ratio of 0.7.

In all the filamentary regions, there is a higher concentration of Class I sources along the filaments. This could be because reddened Class II sources appear as Class I sources or because there are actually more Class I sources. These filaments of dark clouds could be the precursors of massive star formation and progenitors of young clusters, as noted in previous studies. The catalogue of IRDCs taken from Peretto & Fuller (2009) in the same latitude–longitude range is used to ascertain whether the IRDCs and YSOs are co-located. When positional matching is carried out between YSOs and IRDCs, their central coordinates do not match within 2-arcsec separation. However, we see the association of YSOs and IRDCs from a 3-arcsec separation onwards. In order to quantify the association of YSOs with the known IRDCs, we computed the distance of Class I/II sources from the IRDCs. The histogram in Fig. 3 gives a summary of this estimate for all the IRDCs. Up to a distance of 90 arcsec from IRDCs, the number of Class I sources is greater than

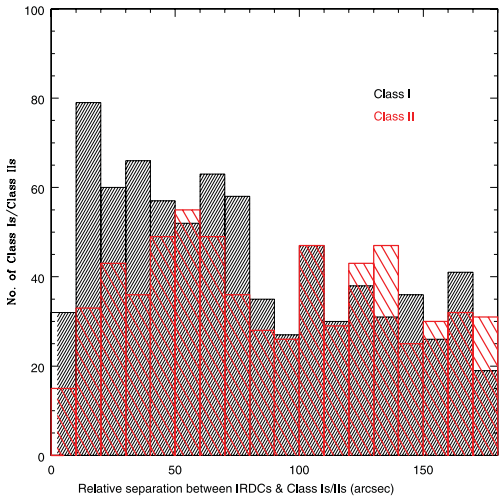

Figure 3. Histogram showing the relative separation of infrared dark cloud (IRDC) centres and Class I/II sources. A greater number of Class I sources are associated with IRDCs than Class IIs for smaller angular separations.

the number of Class II sources. Beyond this, the numbers of Class I and Class II sources are similar. Peretto & Fuller (2009) gives the physical extent of each of the IRDCs, which is greater than 5 arcsec (usually in the range 30–50 arcsec; in some cases more than 200 arcsec). Hence, it can be assumed that at least some of the YSOs are associated with the same region as where the IRDCs are found. In general, wherever we find a high density of Class I sources, the number of IRDCs is also found to be greater. This once again proves that the filamentary regions identified here are probable sites of high-mass star formation.

3.3 Distances

The south-west region of M17, $9^\circ < l < 14^\circ$, $-0.2^\circ < b < -0.45^\circ$, is termed the 3-kpc arm (Rougoor & Oort 1960; Clemens et al. 1986) and contains several molecular clouds, with the near 3-kpc arm at a distance of 5.2 kpc from the Sun. Most of the star formation studies in the 3-kpc arm are focused on the other end of the arm, which extends in the l range 340°–360° (4th Galactic quadrant). The association of the filamentary structures in our study with the near 3-kpc arm has been checked by comparison with other studies in this region. For sources to be physically associated, they have to be coherent in lbv space. The latitude range $10^\circ < l < 15^\circ$ has several spiral arms crossing over in the Galaxy, and the velocity measurements in this l range will give ambiguous results. Although our region of study is an extension of M17SWex in l–b space, it is closer to the Galactic plane (b is lower compared with M17 and M17Swex). We therefore assume that this region is not physically associated with the Sagittarius arm, but might be part of other inner arms. M17 and M17SWex are at a distance of 2.1 kpc in the Sagittarius arm (Povich & Whitney 2010). The previous distance estimations towards W31 and W33 star forming regions give a range of values (3.3–7 kpc towards W31 and 2.4–7 kpc towards W33). Keeping aside the distance ambiguity, the study of this region is of importance as it can give insights into initial states and characteristics of the formation of massive stars, OB associations and stellar clusters.

Because the uncertainty related to distance exists for the identified sources in the entire region, while fitting SEDs we have given a common distance range of 4–6 kpc in the input of the SED fitting tool, except for regions 1 and 2 and for region 9, which have 2.1 kpc (Povich & Whitney 2010) and 3.6 kpc (Henning et al. 2010) respectively, with a ∼10 per cent uncertainty in range (Table 1).

3.4 Spectral energy distribution

In order to characterize the nature of YSOs, we construct SEDs for the Class I and Class II objects identified in the filamentary regions and clusters. We use the online YSO SED fitting tool developed by Robitaille et al. (2007) to estimate the physical properties such as mass, age, accretion rate of discs and envelopes of YSOs. In the Robitaille et al. (2007) models, masses are sampled between 0.1 and 50 $M_\odot$ and ages between 10^3 and 10^7 Myr. For each set of mass and age, the temperature and radius are found by interpolating the pre-main sequence evolutionary tracks of Siess, Dufour & Forestini (2000) and Bernasconi & Maeder (1996). Once the stellar parameters are determined, values of disc and envelope parameters are sampled from ranges that are functions of the evolutionary age of the central source, as well as functions of stellar masses in certain cases. Parameters corresponding to the model that fits the observed flux values with $\chi^2_{\rm min}$ are taken as the YSO parameters. Parameters of models that satisfy the criteria $\chi^2_{\rm min} - \chi^2_{\rm best} < 3$, where χ^2 is the statistical goodness-of-fit parameter per data point, are used to estimate the error in the estimated parameters.

SED analysis was carried out only for 425 Class I and 241 Class II sources, which were detected within the boundaries of the 10 identified regions. We have assumed an A_v range of 1–40 mag for these sources. SEDs were constructed using 2MASS and IRAC magnitudes (wavelength range 0.1–8 μm) for some sources, whereas only

Table 1. Filamentary regions and clusters with their source content.

Region	Name	Distance range[a] (kpc)	Size (arcmin)	Class I	Class II	Number of IRDCs	Methanol masers	IR bubbles	Starless clumps
1	G14.2-0.55	4–6	20	59	57	27	1	-	4
2	G13.87-0.48	1.9–2.3	14	18	20	14	-	1	1
3	G14.62-0.05	1.9–2.3	-	71	54	40	5	3	13
4	G13.26-0.31	4–6	20	17	5	16	-	-	-
5	G13.05-0.15	4–6	33	163	32	40	1	1	∼14
6	G12.8+0.50	4–6	-	21	36	21	1	1	5
7	G12.34+0.51	4–6	8	9	11	10	-	1	-
8	G11.86-0.62	4–6	7.5	7	6	8	1	-	-
9	G11.13-0.13	3.2–3.9	20	34	11	20	1	1	5
10	G10.67-0.21	4–6	9	26	9	20	3	-	1

[a]As given in the input of the SED fitting tool (see Section 3.1).

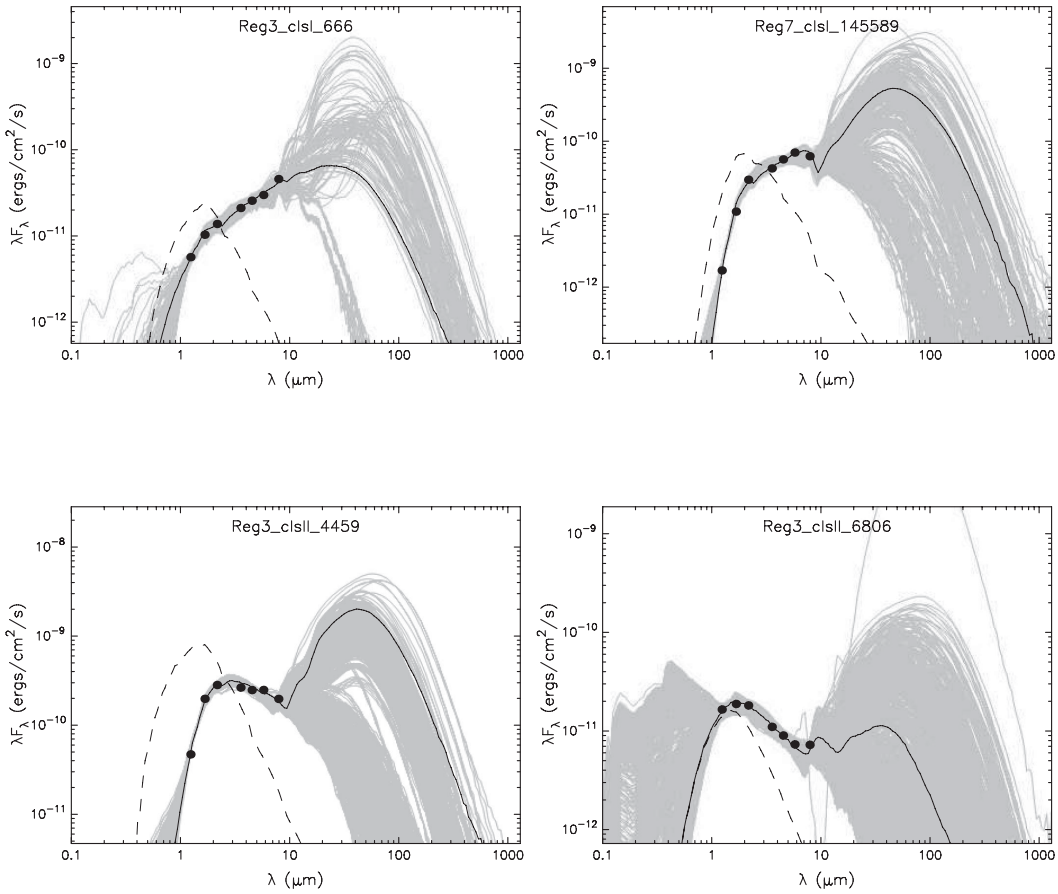

Figure 4. Spectral energy distributions of Class I and Class II sources constructed using JHK_s and IRAC magnitudes. The top two sources are the Class I sources from region 3 and region 7, with ages of 0.004 ± 0.068 and 0.014 ± 0.075 Myr and masses of 2.09 ± 0.3 and $7.14 \pm 0.04\,M_{\odot}$, respectively. The bottom sources are Class II sources from region 3 with ages of 0.469 ± 0.074 Myr, 0.013 ± 0.041 and masses of $4.89 \pm 0.03\,M_{\odot}$, $10.4 \pm 0.05\,M_{\odot}$, respectively.

IRAC magnitudes were considered for other sources. This is because some YSOs have an error of more than 0.1 mag in the 2MASS magnitudes, giving unrealistic SED fittings. This means that for each region a few SEDs are derived from IRAC and 2MASS magnitudes, whereas the remaining SEDs are constructed with IRAC magnitudes only. Fig. 4 shows examples of SEDs of two Class I and two Class II YSOs from different regions. The solid black line shows the best-fitting model, while the grey lines represent models that satisfy the above-mentioned criteria. Among the output parameters, we present the results on mass and age estimates in the next section. The assumptions used in the models affect the reliability/accuracy of estimated parameters, which are considered as inevitable errors that occur in attempts to obtain model dependent parameters. The estimated parameters are based on the data mentioned above and do not include far-IR data. This introduces relatively large errors in the estimated parameters, as suggested by the large number of grey coloured fitted lines in the SED plots. Because Class I sources peak at mid-IR wavelengths, and Class II sources in the near-IR, mass and age estimations based on the near-IR and mid-IR are sufficiently reliable. In the absence of far-IR wavelengths, disc parameters are less constrained and the envelope parameters are highly uncertain. Inclusion of far-IR and submm data will reinforce the disc nature and characteristics of YSOs. Results presented in this study are based on the high-resolution data for a wide sample of candidate YSOs based on combined 2MASS and GLIMPSE data. The relatively poor resolution resulting from the large aperture sizes of longer-wavelength observations needs to be addressed. The inclusion of longer-wavelength data would effectively reduce the detected source density in each region, especially because these are distant star forming regions. Hence, instead of a statistical analysis of the properties of large numbers of Class I/Class II sources, such studies would reduce to individual source studies.

3.5 Parameters of the identified YSOs

The numbers of Class I and Class II sources identified in each region are tabulated in Table 1, along with the number of IRDCs, methanol masers, IR bubbles and starless clumps. A rough size of the filamentary star forming region was measured on each 5.8-μm image using the ruler option in the SAOIMAGE DS9 image display widget. The approximate size (in arcminutes) as well as the distances assumed for each region (see Section 3.3) are also tabulated in Table 1. It is seen that the number of Class I sources roughly scales with the number of starless clumps.

The estimated mass distributions of Class I and Class II sources in the 10 identified regions are shown in Fig. 5. The histograms presented in Figs 5 and 6 may be strongly influenced by an incomplete census of YSOs. This study is likely to have missed a number of low-mass objects, and the observations are more sensitive to (low-mass) Class II objects than Class I objects. It can be seen that Class I sources are found to have a range in mass such that most of them have mass $\geq 8\,M_{\odot}$. The upper mass limit in most of the region is found to be 30–32 $M_{\odot}$, although there are a few massive sources. The most massive YSOs in our study are found

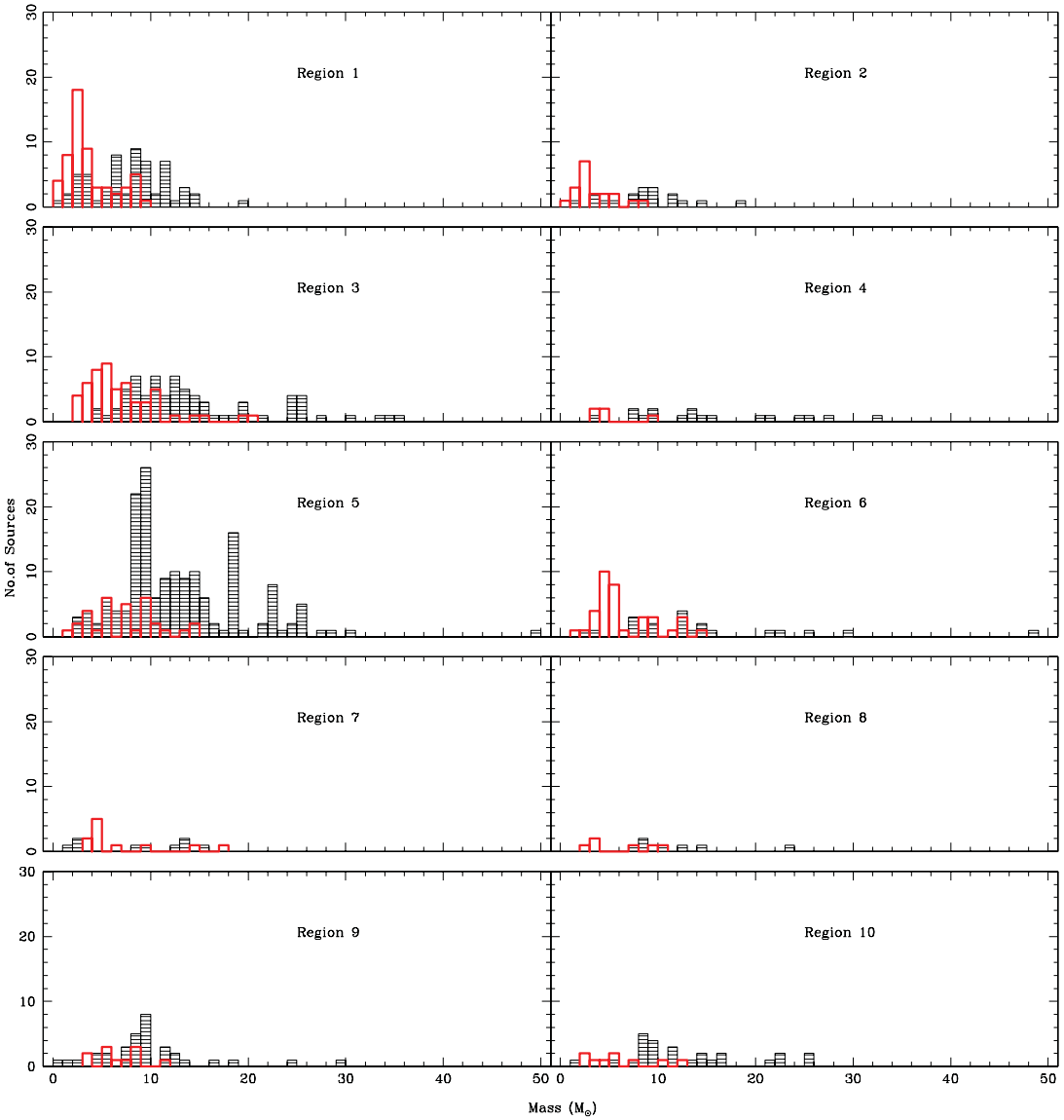

Figure 5. The mass distribution of Class I sources (black striped blocks) and Class II sources (red blocks) identified in 10 regions.

in regions 5 and 6. Among the Class I sources, eight sources have estimated mass $>30\,M_\odot$; four of them are in region 3, one source is in region 4, two are in region 5 and one source is in region 6. Six of them are in the mass range 30–36 $M_\odot$, while two are in the range 48–50 $M_\odot$, the latter being the most massive ones in this study. This suggests that the regions studied here are indeed forming massive stars. Region 5 has the highest ratio of massive Class I to Class II sources. Regions 1 and 2 are found to have more low-mass sources, whereas region 6 has more sources in the high-mass range.

The mass distribution shows that for all the regions there is a significant reduction in the number of Class II sources with mass greater than $8\,M_\odot$, while most of the Class I sources have masses greater than $8\,M_\odot$. The number of Class I sources in the mass range $< 6\,M_\odot$ is relatively lower, where we can see large number of Class II sources. This may be due not to the lack of Class I sources with $<6\,M_\odot$ mass, but to the detection limit. Observational evidence for lower-mass protostars is difficult to obtain. As high-mass protostars are much more luminous than lower-mass protostars, they are far easier to detect. In the Class II phase we do find a higher fraction of lower-mass protostars, as such sources are more identifiable in this phase. Region 1 is found to have a relatively large number of low-mass Class I sources, and this may be because this region is closer, being part of M17SWex.

The estimated age distributions of Class I and II sources in the 10 identified regions are shown in Fig. 6. Most of the Class I and Class II sources are of age $\leq$0.1 Myr. In all regions, Class II sources have a larger range in age, with some sources as old as 3 Myr. The age distribution for Class II sources shows that in some regions star formation started $\sim$3 Myr ago, and continued until the Class I and Class II sources started forming together in the last $\leq$0.5 Myr. Most of the Class I and II sources are found to have formed in the last 0.1–0.5 Myr. Regions 1, 3 and 6 show a more or less continuous formation of Class I sources with ages up to $\sim$2.2 Myr.

3.6 Star formation in filaments and clusters

The description of eight filamentary star formation sites and two candidate clusters of Class I and Class II objects, including their observed structural details, YSO content and other associated sources, are given below.

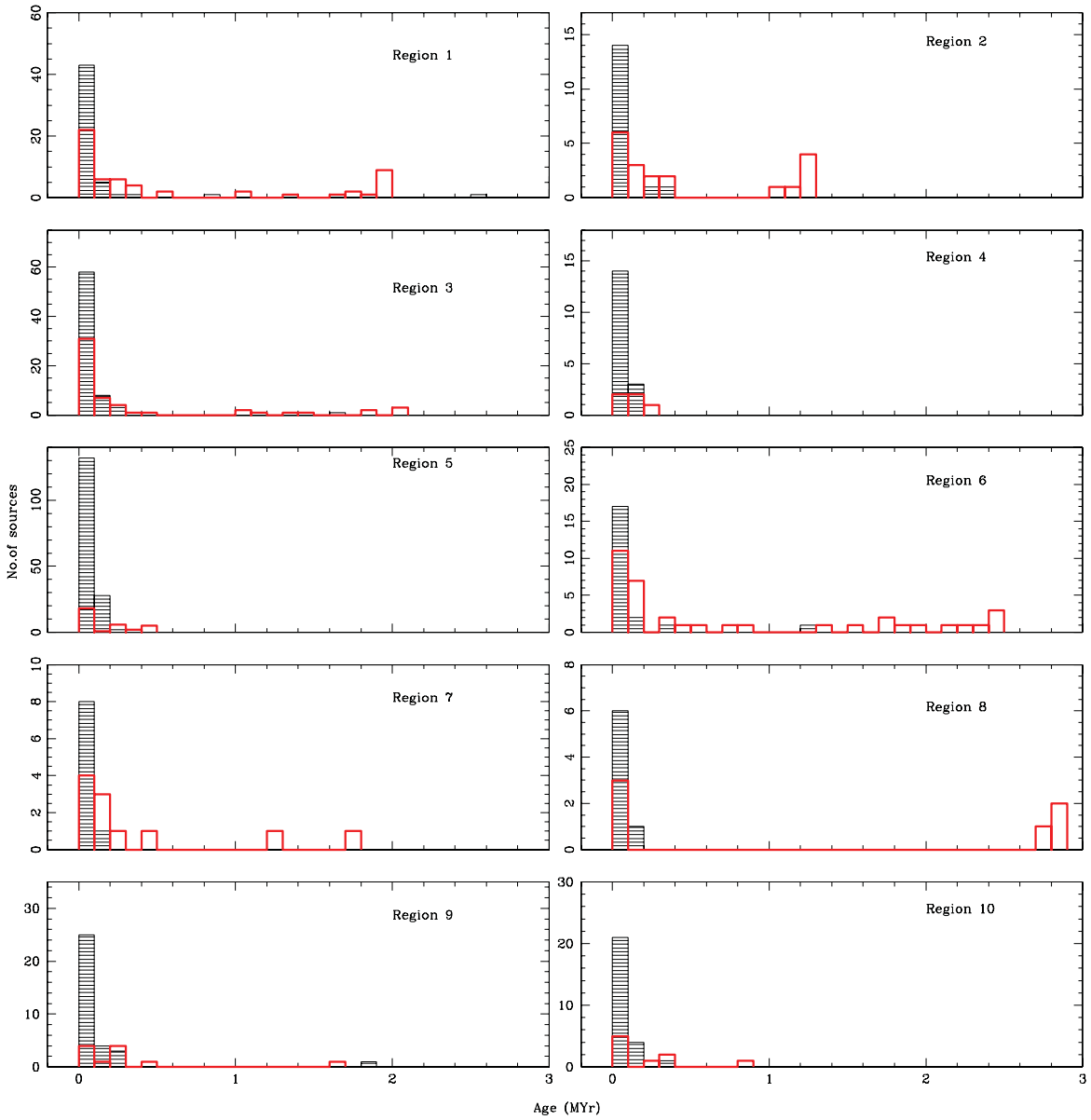

Figure 6. The age distribution of Class I sources (black striped blocks) and Class II sources (red blocks) identified in 10 regions.

(1) G14.2-0.55 (region 1 – Fig. 7)
This region is part of M17SWex, which extends ∼50 pc south-west from the Galactic H II region M17. Povich & Whitney (2010) carried out a census of young stellar content using 2MASS, GLIMPSE, MIPSGAL and MSX data and detected >200 YSOs forming B stars. For the 64 820 GLIMPSE sources located within a $1^{\circ} \times 0.^{\circ}75$ field encompassing M17SWex, Kurucz (1993)-reddened stellar atmospheres were fitted, and those sources with a poor fit were considered as possible YSOs by Povich & Whitney (2010). From these, sources with IR excess emission were filtered out using Smith et al. (2010) colour criteria, and AGB contaminants were removed by applying Whitney et al. (2008) colour criteria. Assuming that M17SWex will form an OB association with a Salpeter initial mass function, they suggested (i) more rapid circumstellar disc evolution in more massive YSOs, and (ii) a delayed onset of massive star formation in this region. We do not study the entire M17Swex region, but a major part of the filamentary dark clouds, which are termed region 1 and region 2. Our study looks at the general trend in mass and age for YSOs that are detected in or near the filamentary dark clouds.

The distribution of Class I sources follows a pattern identical to that of the structure of dark filaments, giving the impression that they are co-located, while most of the Class II sources are not closely associated with the filamentary structure. Instead of a single elongated hub, many tiny filaments are oriented in the decreasing longitude direction (away from M17), giving the appearance of an elongated dark filament. For a distance of 2.1 kpc (Povich & Whitney 2010) we estimate a length of ∼12 pc for this filament, corresponding to a size of 20 arcmin. Class II sources show a peak in mass at around 2–3 $M_{\odot}$, and Class I sources peak at 8–9 $M_{\odot}$. Class I sources also show a distribution in mass up to 15–20 $M_{\odot}$, while Class II sources have masses only up to 10 $M_{\odot}$. From the age distribution of Class I and Class II sources, it can be seen that most sources formed ≤0.1 Myr ago. Some of the Class II sources have ages up to 2 Myr, while most of the Class I sources have age ≤0.2 Myr. The star formation processes are found to have

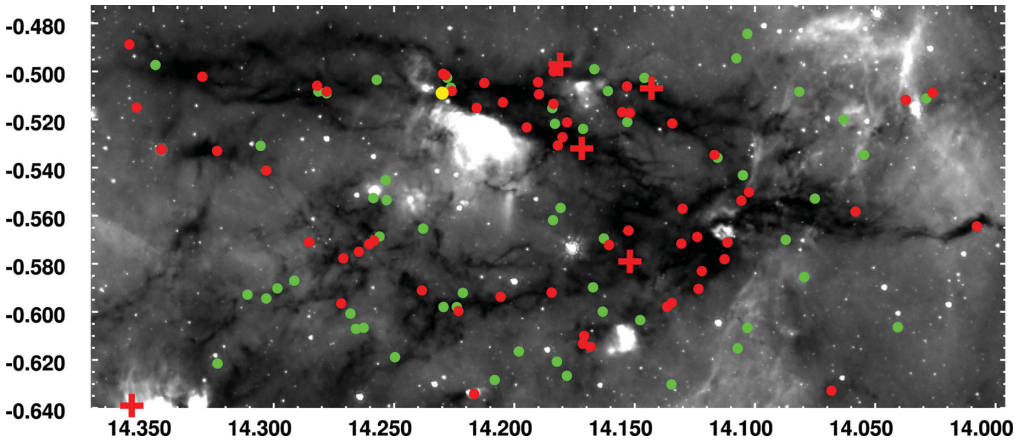

Figure 7. G14.2-0.55 (region 1). Class I sources are shown as red circles and Class II sources as green circles. Only those YSOs considered for spectral energy distribution fitting are shown. The locations of tracers such as masers and starless clumps are also marked as follows: yellow, masers (without distance information); blue, near 3-kpc arm masers; magenta, far 3-kpc arm masers; red crosses, starless clumps with near distance solutions assumed; red diamonds, starless clumps with far solutions.

started around 2 Myr ago, as evident from the presence of almost 10 Class II sources as old as 2 Myr (Fig. 6). The star formation has continued and produced a maximum number of both Class I and Class II sources forming together ∼0.1 Myr ago. In agreement with Povich & Whitney (2010), we also detect an increased formation of YSOs, after a delay of ∼2 Myr in this region.

(2) G13.87-0.48 (region 2 – Fig. 8)

This region is also part of M17SWex and has been studied by Povich & Whitney (2010). For a distance of 2.1 kpc towards this region we estimate a length of ∼8.5 pc for this filament, corresponding to a size of 14 arcmin for the filamentary structure. Similar trends in the pattern of Class I and II sources to those noted in region 1 are seen here. The distribution of mass of Class I/II sources does not show a substantial difference from those noted in region 1. The presence of elongated hubs can be seen here, although the tiny filaments are not obvious. Here Class II sources started forming at around 1.6 Myr ago, and star formation processes peaked in the last 0.1 Myr, with most of the Class I and Class II forming together. Thus we find that region 2 also has older Class II sources, but only younger Class I sources. Furthermore, Class II sources are found to be younger than those in region 1, suggesting that the formation in region 2 started later, by about 0.4 Myr. This might support the suggestion of sequential star formation in the M17 complex.

(3) G14.62-0.05 (region 3 – Fig. 9)

Along with IRDCs and starless cores, mid-IR nebulosity is also seen in this latitude–longitude range. We identify this region as a candidate cluster of Class I and II sources. Highly luminous background emission and the absence of definite filamentary structure indicate that this region is more evolved than the others. Class I sources are located mainly in the dark patches. Class I sources show a peak in the mass distribution at 8–13 $M_{\odot}$ and range up to 30 $M_{\odot}$. The mass distribution of the Class II sources peaks at 5–6 $M_{\odot}$. No Class I source with mass $< 4\,M_{\odot}$ is seen. Only very few Class II sources have mass $>10\,M_{\odot}$, whereas a substantial number of Class I sources exist in the 10–30 $M_{\odot}$ mass bin. Both Class I and Class II sources peak at age $\leq$0.1 Myr. Some of the Class II sources are older, up to 2.1 Myr. Similar to regions 1 and 2, this region also shows that most of the YSOs formed about 2 Myr after the initial star formation. There are four Class I sources with mass $>30\,M_{\odot}$ in this region; with masses 30.74 ± 1.67,

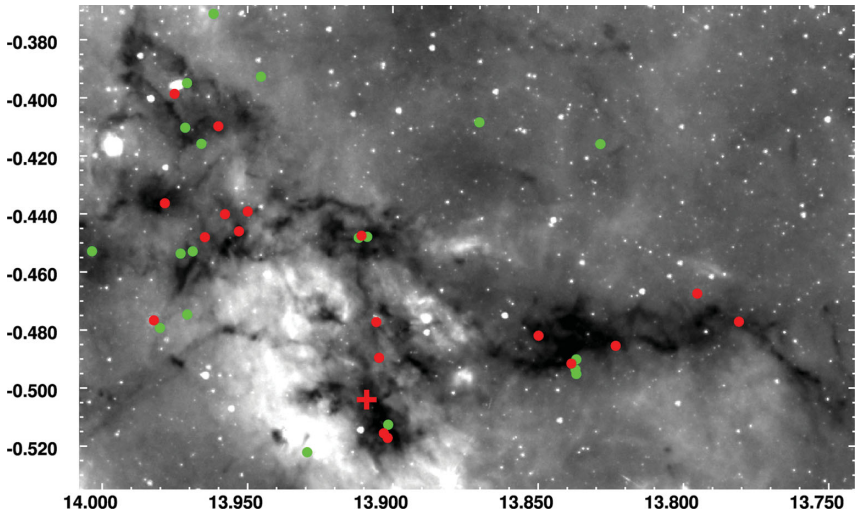

Figure 8. G13.87-0.48 (region 2). Symbols as in Fig. 7.

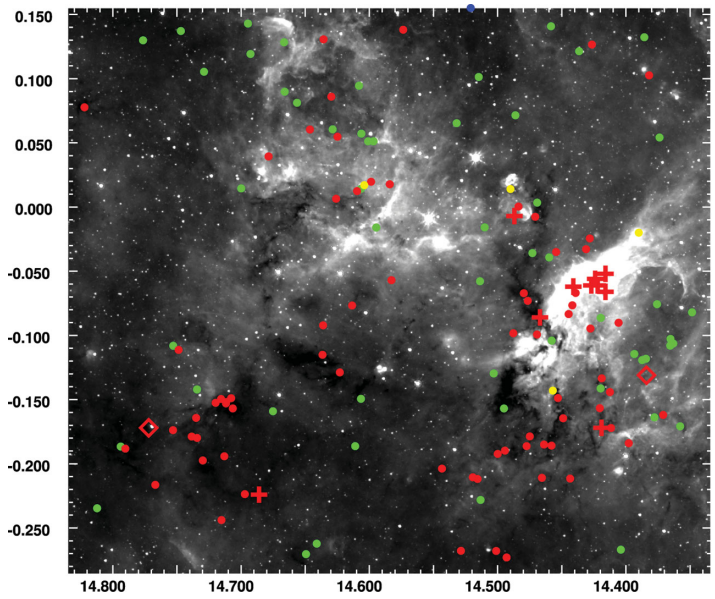

Figure 9. G14.62-0.05 (region 3). Symbols as in Fig. 7.

33.92 ± 0.45, 34.49 ± 1.5 and 35.78 ± 10.75 $M_{\odot}$, the last one showing the highest error in estimated mass among all YSOs.

(4) G13.26-0.31 (region 4 – Fig. 10)
This region consists of a network of tiny filaments, seen inclined to the general Galactic plane and parallel to region 5, which is located at a higher *b* value. The length of the structure is ∼20 arcmin, stretching from G13.15-0.38 to G13.4-0.24, and corresponds to a physical length-scale in the range 23–34 pc for the adopted range of distance (4–6 kpc). The increased number of Class I sources above Class IIs suggests that this region may be hosting a very recent star formation site. All Class I sources have age ≤0.1 Myr, while Class II sources are slightly older, up to 0.3 Myr. Hence, unlike regions 1 and 2, we detect only recent star formation activity in this region. Most of the Class II sources have mass in the range 3–5 $M_{\odot}$. A greater number of Class I sources are seen in the 7–10 $M_{\odot}$ and 13–14 $M_{\odot}$ mass bins. This region also hosts a Class I source with mass 32.4 ± 4.07 $M_{\odot}$. This region is located close to W33, similar to region 5. Signatures of HFSs with tiny filaments arising parallel to the short axis of the hub are observed in this region. At some points the filaments are entangled where greater numbers of Class I sources are located. The filaments in this region are likely to be created by the outflows/winds from W33.

(5) G13.05-0.15 (region 5 – Fig. 11)
This is one of the prominent regions located near the W33 complex, where we can see Class I sources closely associated with the filamentary structure. This is the longest filamentary structure, with a size of ∼33 arcmin (corresponding to a physical length in the range 38–56 pc according to the distance adopted). It is located to the south-east of the W33 complex and is inclined with respect to the Galactic plane. A long strand of dark filament with tiny filaments branching out at some points and entangled together at some points gives the impression of a HFS.

The greater number of Class I sources compared with Class II sources and the presence of a large number of IRDCs along with the morphology of the filaments suggest that the region is highly primitive and harbours a stellar nursery. The comparatively evolved

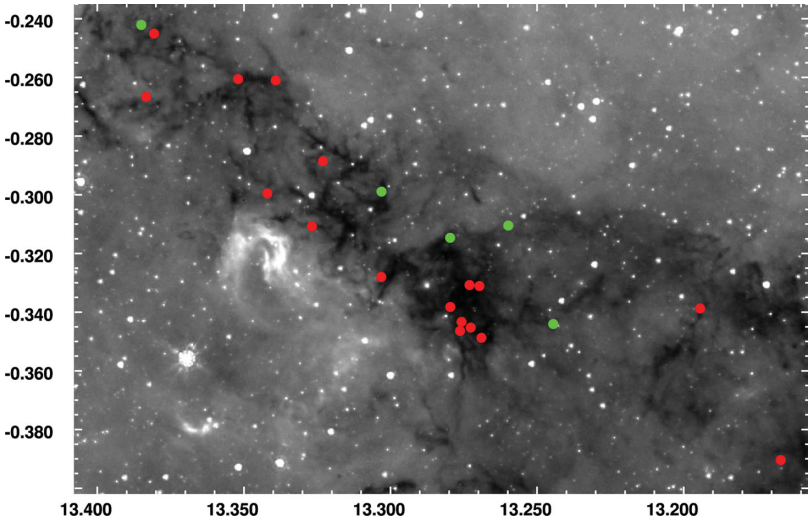

Figure 10. G13.26-0.31 (region 4). Symbols as in Fig. 7.

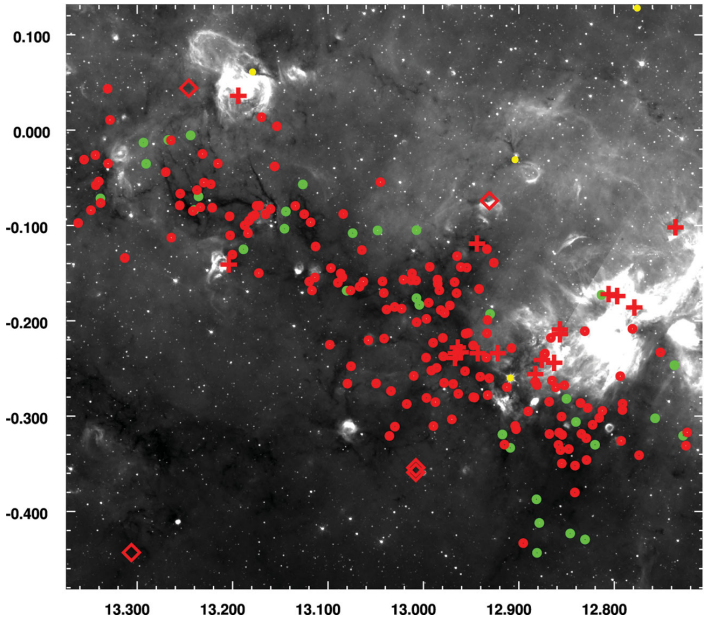

Figure 11. G13.05-0.15 (region 5). Symbols as in Fig. 7.

ultra-compact H II region, W33, should be influencing the structure as well as star formation in this region. The Class I sources are seen to be nicely aligned along the length of filaments, which extend from G12.8-0.35 to G13.3-0.00, as seen in Fig. 11. The mass distribution of Class I sources shows a peak at 9–10 $M_\odot$. A significant fraction of Class I sources have mass >8 $M_\odot$, indicating that this region is prolifically forming high-mass stars. There are two Class I sources with mass greater than 30 $M_\odot$, namely with masses 30.74 ± 1.06 $M_\odot$ and 49.21 ± 2.82 $M_\odot$. Thus this region hosts the most massive YSO detected in this study. Only a very few Class II sources have mass higher than 10 $M_\odot$. It is found that both Class I and Class II sources have age ≤0.1 Myr, with some of the Class II sources as old as 0.5 Myr. Similarly to the star formation regime in region 4, this region also has started forming stars very recently.

(6) G12.8+0.50 (region 6 – Fig. 12)
The region is abundant in Class II sources and dust-lane emissions compared with the other regions and is classified as a candidate cluster. This is the only region where we find a significantly greater number of Class II sources than that of Class I sources. Most of the Class II sources have mass in the 4–6 $M_\odot$ range, while most Class I sources have mass up to 16 $M_\odot$, with a very few ranging up to 30 $M_\odot$. Class I sources have age ≤0.1 Myr, whereas Class II sources are as old as 2.5 Myr. The Class II sources are found to be forming from 2.5 Myr until now, whereas the high-mass stars are forming only now. The region hosts the second highest massive YSO detected in our study, with a mass of 48.74 ± 1.04 $M_\odot$. The structure and star formation in this region are possibly modified by either the W33 region or the sites of star formation seen in dust emission.

(7) G12.34+0.51 (region 7 – Fig. 13)
This region, which has relatively faint features compared with other regions, consists of a filamentary structure with tiny filaments branching out forming a HFS. The filaments can be seen emerging out of two regions that show dust emission, representing the hub. The filaments are found to be aligned in the same direction. The 8-arcmin size of this region corresponds to a length-scale of

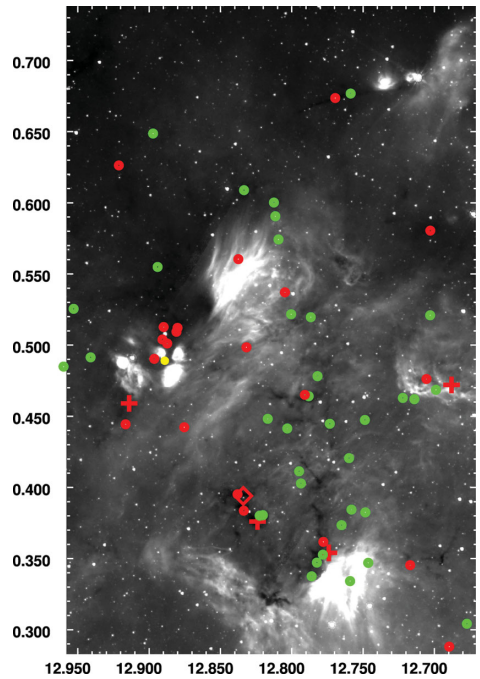

Figure 12. G12.8+0.50 (region 6). Symbols as in Fig. 7.

9–14 pc for the 4–6 kpc adopted distance range. We detect only a small number of Class I and II sources in this region. Class II sources show a peak in mass in the range 5–6 $M_\odot$, and Class I sources vary up to 16 $M_\odot$. Both Class I and Class II sources have an age ≤0.1 Myr, but some Class II sources are as old as 1.8 Myr. As the Class I sources are not found in most parts of the filaments, it appears that the filaments in this region have not attained the critical mass to start star formation.

(8) G11.86-0.62 (region 8 – Fig. 14)
This region has the same pattern as that of region 7. Here, also, signatures of a HFS can be seen. The branching out of filaments

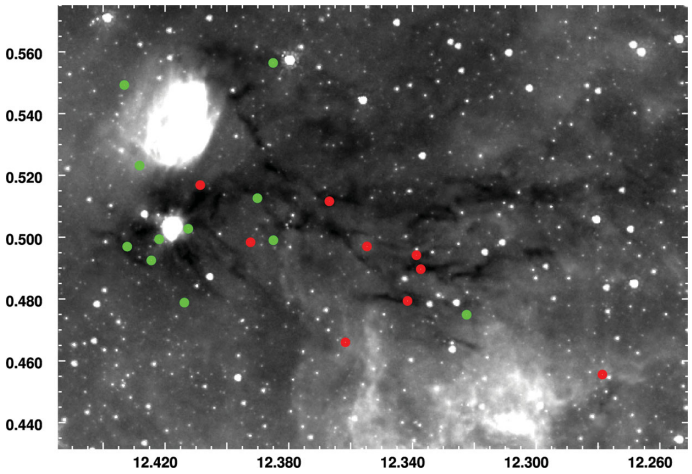

Figure 13. G12.34+0.51 (region 7). Symbols as in Fig. 7.

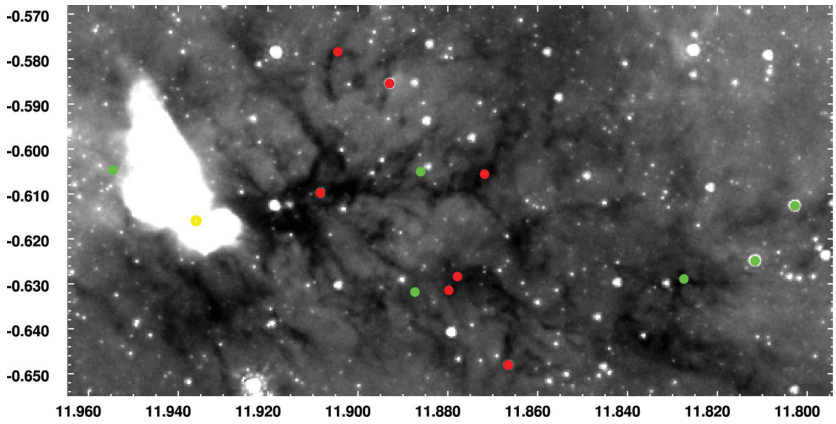

Figure 14. G11.86-0.62 (region 8). Symbols as in Fig. 7.

to form a network is clearly observable in this region. For the adopted distance range, we estimate a length of 8.7–13 pc, corresponding to the 7.5-arcmin size of the filamentary structure. There are no Class I sources with mass $<7\,M_{\odot}$, and most of them are in the range 8–9 $M_{\odot}$. Masses of Class II sources vary from 2 to 11 $M_{\odot}$. Most of the Class I and Class II sources have ages $\leq$0.1 Myr. A few of the Class II have ages in the range 2.7–2.9 Myr.

(9) G11.13-0.13 (region 9 – Fig. 15)

This is one of the well-studied filamentary IRDCs. Carey et al. (1998) confirmed the presence of dense molecular gas in this cloud using millimetre spectral lines of H_2CO. Carey et al. (2000) present the 850- and 450-μm continuum images from SCUBA observations and postulate the presence of the early stages of star formation within the cloud. Johnstone et al. (2003) demonstrated the underlying radial structure of the cloud using 850-μm observations, and according to their findings this is the first molecular filament observed to have a radial profile similar to that of a non-magnetic isothermal cylinder. Henning et al. (2010) made use of *Herschel* data to detect the embedded population of pre- and protostellar cores in this cloud. Out of the 18 cores they characterized using SED analysis, two have masses over 50 $M_{\odot}$, implying the presence of massive star formation. The presence of high-mass star formation in the cloud has also been noted by other authors: Chen et al. (2010) (the presence of EGOs as tracers), Pillai et al. (2006) (water and methanol emission) and Gomez et al. (2011) (using methanol emission).

A distinct filamentary cloud structure with tiny filaments originating at various points is seen here. It is interesting to note that Class I sources are aligned along the string of filamentary structure, while Class II sources are located more or less distant from the main filament. The approximate size of the filament is ∼20 arcmin. This corresponds to a length of ∼21 pc for a distance of 3.6 kpc to this region. Most of the Class I sources have mass $<10\,M_{\odot}$ and age $\leq$0.1 Myr, with a peak distribution in mass at 9–10 $M_{\odot}$, and a very few range up to 30 $M_{\odot}$. Many Class II sources have mass in the range 5–9 $M_{\odot}$ and age ranges to 0.5 Myr. Many IRDCs, starless clumps (five with a near distance solution), one maser source and one IR bubble are seen at this location. IRDCs are also nicely aligned in these filaments. Most of the star formation in this region is found to be in the last 0.5 Myr.

(10) G10.67-0.21 (region 10 – Fig. 16)

Tiny filaments emanating from smaller round hubs are grouped to make a clustered form of filaments in this region. This region with a size of 9 arcmin corresponds to a length-scale in the range 10–16 pc for the adopted distance range of 4–6 kpc. Most of the Class I and Class II sources have an age $\leq$0.1 Myr. Masses of Class I sources vary up to 26 $M_{\odot}$, with many peaking at 8–9 $M_{\odot}$. Class II sources

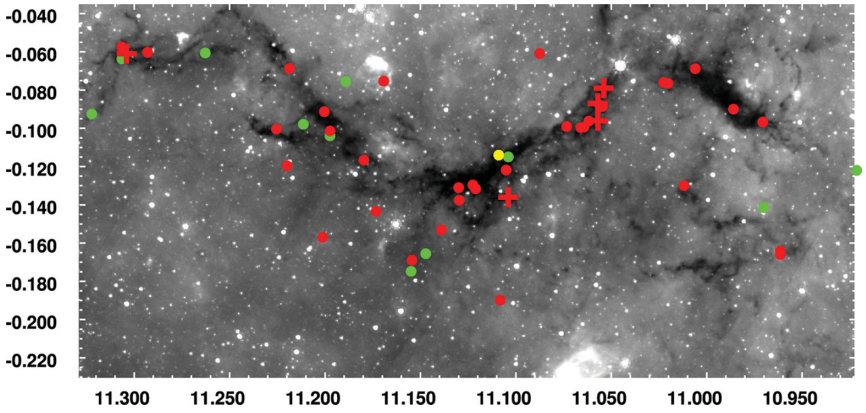

Figure 15. G11.13-0.13 (region 9). Symbols as in Fig. 7.

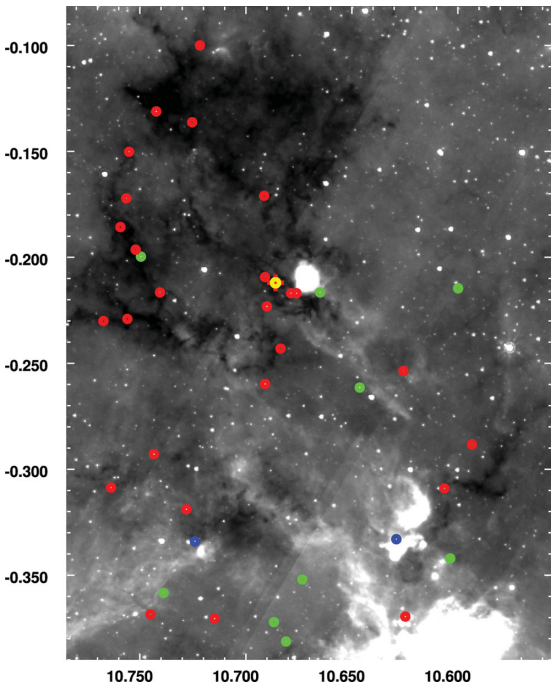

Figure 16. G10.67-0.21 (region 10). Symbols as in Fig. 7.

have masses in the range 2–13 $M_\odot$. This is a site experiencing star formation in the last 0.5 Myr.

4 DISCUSSION

We have studied YSOs in 10 star forming regions in the inner Galaxy. The presence of massive Class I sources along with other tracers of high-mass star formation prove that these are sites of high-mass star formation. The regions show filamentary dust lanes, and Class I sources are found to be preferentially located along them. As these regions are located near well-known H II regions, the structure and star formation in these regions may be dictated by them.

Fig. 17 shows the locations of tracers of high-mass star formation such as IRDCs, masers, starless clumps, IR bubbles/H II regions, radio sources, EGOs and HMPOs identified in the Galactic region of our study. Although the 10 regions studied here were selected based on the density of the Class I and Class II sources, a few other concentrations of the above-mentioned tracers can be identified in this plot. Thus, Fig. 17 shows the locations of these concentrations and suggests that there may be a few more high-mass star forming sites close to the regions studied here. We do not study them, as we detected only a few Class I sources in these regions. It is possible that these regions are in the very early stage of star formation. The presence of such regions once again strengthens the argument that this part of the Galaxy is undergoing high-mass star formation, and these regions are potential targets for further studies.

Out of the 10 regions studied here, four (regions 1, 2, 3 and 6) show signatures of delayed star formation. Although our results suggest a delay in the formation of Class I sources (massive stars), this is only indicative because of the incompleteness in the data of Class II sources. Regions 1, 2 and 3 are located close to M17SWex. There is an indication of sequential star formation in this region owing to the effect of M17SWex. Six regions (regions 4, 5, 7, 8, 9 and 10) were found to be forming high- and low-mass stars together. Stars have been forming in these regions for the last 0.5 Myr.

Fig. 18 shows the plot of age versus mass for the Class I and Class II sources with estimated errors in masses and ages. In the plots we have truncated the limits on both the *x*- and the *y*-axis, including most of the sources while excluding the extreme ones. The interpretations of this plot are likely to be affected by the incomplete number of observed YSOs in the region. Furthermore, the errors on many of the masses and ages are greater than the predicted values themselves. In the case of Class I sources, the plot is shown only up to 1 Myr, although there are 13 sources with ages greater than 1 Myr and up to 8 Myr having mass less than 8 $M_\odot$. It is possible that these older Class I sources may be Class II sources viewed edge-on, through their discs. Most of the Class I sources detected in the regions are found to be younger than 0.5 Myr, and this plot helps us to understand the mass distribution of this population.

The masses of Class I sources were found to be between 2 and 32 $M_\odot$, with most of the sources more massive than 8 $M_\odot$. Thus, high-mass stars have been formed in these regions in the last 0.5 Myr. It can be seen that the relatively low-mass Class I sources have ages up to 0.5 Myr, whereas the more massive sources are younger than 0.2 Myr. It is well known that massive stars form much more quickly than their low-mass counterparts. One would therefore not expect to see massive Class I sources with ages greater than a few tenths of a Myr. The left-hand plot in Fig. 18 supports this theory. The Class II sources are formed in the age range 0–3 Myr, but most of the sources have ages $\leq$0.6 Myr. There are about 20 sources that are older than 3 Myr, up to 10 Myr, and having masses less than 5 $M_\odot$. This suggests that most of the Class II sources have a similar age range to the Class I sources. The mass range

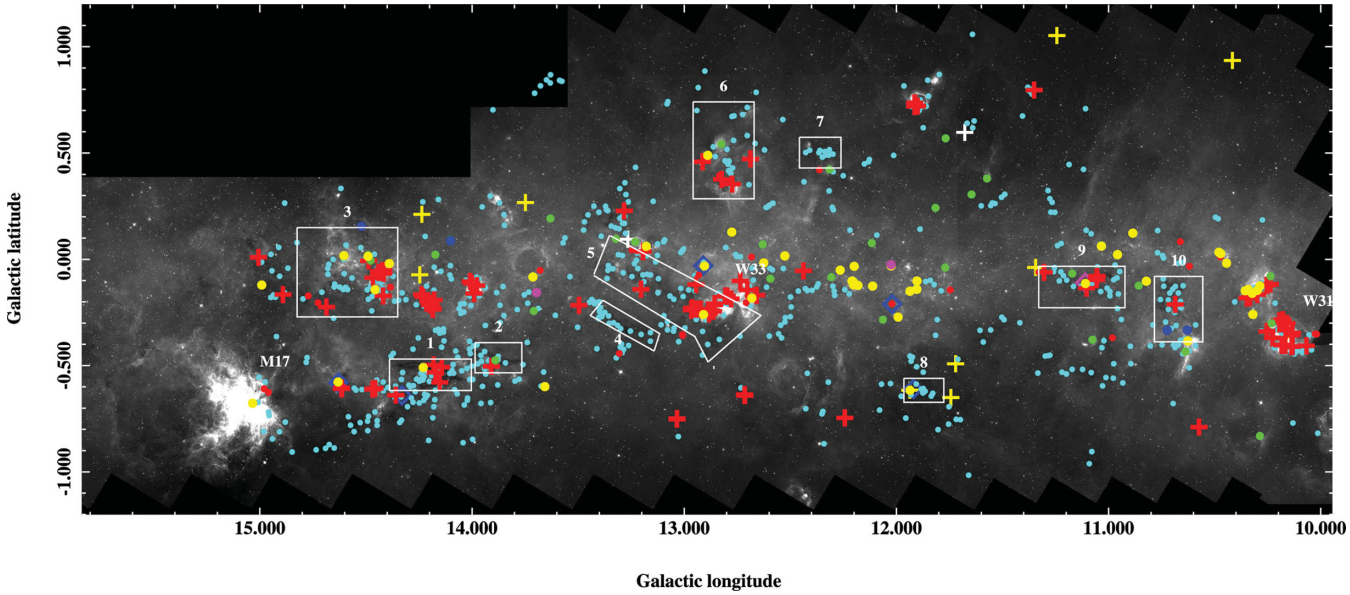

Figure 17. GLIMPSE 5.8-μm image of the entire region with the locations of sources that are used as tracers of massive star formation and distance information in our study. Circles: cyan, infrared dark clouds (IRDCs); green, IR bubbles/H II regions; yellow, masers; blue, near 3-kpc arm masers; magenta, far 3-kpc arm masers; red crosses, starless clumps with near distance solutions assumed; red circles, starless clumps with far solutions; blue diamonds, 'likely' massive young stellar objects (MYSOs); magenta diamonds, 'possible' MYSOs; white crosses: high-mass protostellar objects (HMPOs); yellow crosses, radio sources.

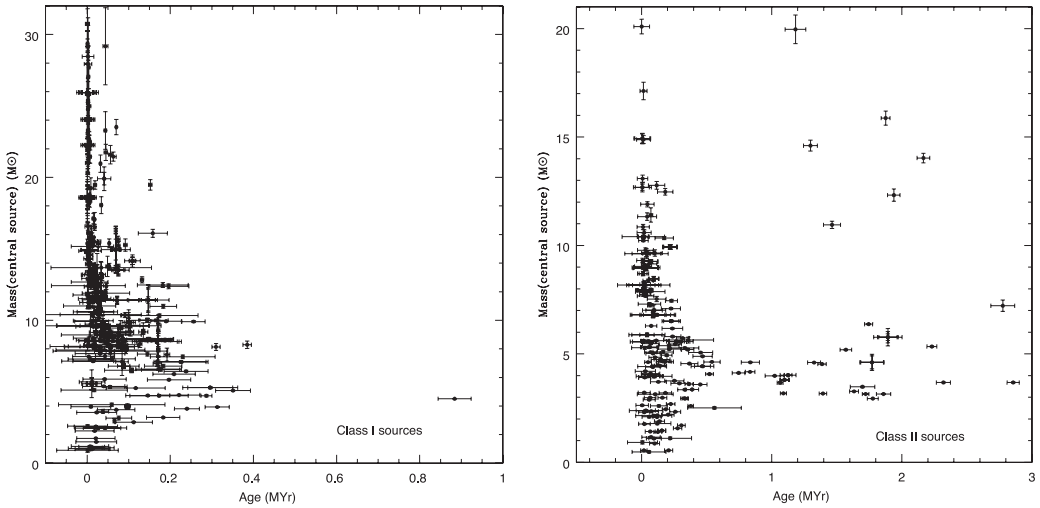

Figure 18. Mass and age distribution of sources in the entire region. The central black dots correspond to the estimated mass and age of each of the young stellar objects. Standard deviations in estimated age and mass are shown as vectors along the *x*- and *y*-axis, respectively.

of the Class II sources is found to be 0.5–20 $M_{\odot}$, but most of the sources have mass lower than 10–12 $M_{\odot}$. Most of the older Class II sources were found to have a mass lower than 8 $M_{\odot}$, except for a few massive sources. The above numbers are only suggestive and could be affected by the incompleteness in the data. We do still find that many (in some regions most) of the Class II sources appear to be as young as the Class I sources. This could be due either to observational bias towards massive YSOs that evolve more rapidly than their low-mass counterparts or to some of the Class II sources being misidentified as Class I sources in the colour–colour analysis because of their orientation (i.e. being viewed pole-on). The environment around each source, the orientation of the source with respect to the observer and the mass of the central object can alter the observed differences in colours and SEDs of Class I and Class II evolutionary stage objects, thereby affecting the properties estimated for them, and can be the reason for obtaining large populations of very young Class II sources. Apart from these biases in the classification of the YSOs, this study supports the evolution of Class I sources into Class II sources.

In summary, we detect YSOs in the mass range 0.5–31 $M_{\odot}$ and in the ∼0.1–3 Myr age range, with most of them in the ≤0.5 Myr age range. These regions thus prove to be abundant in MYSOs in the early stages of formation, pointing to their potential for further studies. One of the regions studied here is found to have a large number of high-mass Class I sources, suggesting that this region (region 5) is forming a massive and rich cluster of high-mass stars.

We observe a HFS in most of the early star forming complexes of filamentary IRDCs. In most cases elongated hubs are seen with tiny filaments. We see various orientations of filaments with respect to the central hub, for example the filaments parallel to the hub or

the filaments radiating in different directions, and in some cases the filaments are entangled. Myers (2009) explains various models of the formation mechanism of HFSs. Analysis of each filamentary star formation site and their environment can lead to an understanding of the formation scenario of HFSs. The filamentary regions are located in the vicinity of massive H II regions, suggesting that the filamentary features could be created as a result of these nearby H II regions. Our regions are located at various distances from the H II regions, and some are located relatively far away. Furthermore, some of these regions are found to host star formation up to 3 Myr ago, with the formation of low-mass stars. Thus, the early formation of small numbers of low-mass stars is not found to destroy the filaments.

The study of star formation in filamentary structures is an emerging area of scientific interest, as new space missions such as *Herschel* and other submm observations have recently detected complex systems of filamentary structures. This information has revolutionized the previous theory of star formation, namely that only self-accreting molecular clouds of circular shape take part in star formation. We have shown that the GLIMPSE data and images are able to identify filamentary structures and thereby contribute to an understanding of the origin and geometry of early star forming processes.

5 CONCLUSION

The major findings of our study can be summarized as follows.

(i) We have identified 1107 Class I and 1566 Class II sources in the Galactic region $10^\circ < l < 15^\circ$, $-1^\circ < b < 1^\circ$.

(ii) We have identified eight early star forming sites of filamentary structures and two candidate clusters of Class I and Class II YSOs. Class I sources are closely associated with the IR dark filaments, while Class II sources are located randomly in these regions. All these sites are found to be co-located with other high-mass star forming tracers.

(iii) In all the regions identified, the observed Class I sources are of age $\leq$0.5 Myr, while Class II sources have ages in the range $\sim$0.1–3 Myr. The majority of the Class I sources are $\geq 8\,M_\odot$, while Class II sources are in the 0.5–10 $M_\odot$ mass range. Low-mass objects are incomplete in this group owing to low flux levels.

(iv) Four of the regions studied are found to show a delay in the formation of most of the YSOs. Our analysis supports the sequential star formation of the M17SWex complex, as suggested previously.

(v) Filamentary and hub–filamentary features are found in most of these regions, and harbour star formation in the $\sim$0.1–3 Myr age range. The lengths of the identified filaments are estimated as 8–33 arcmin ($\sim$9–56 pc).

(vi) This study brings into focus 10 sites of massive star formation in the inner Galaxy, harbouring very young YSOs. We suggest that these are potential targets for understanding the formation and evolution of massive YSOs.

ACKNOWLEDGEMENTS

We thank the anonymous referee for useful comments and suggestions, which helped to improve the paper. BB gratefully acknowledges the University Grants Commission, New Delhi, for financial support through the RFSMS Scheme, and the Indian Institute of Astrophysics, Bangalore, where most of this work was done, for hospitality. This research has made use of data products from the GLIMPSE survey, which is a legacy science program of the *Spitzer* Space Telescope funded by the National Aeronautics and Space Administration, and also of data products from the Two Micron All Sky Survey (2MASS), which is a joint project of the University of Massachusetts and the Infrared Processing and Analysis Center/California Institute of Technology, funded by the National Aeronautics and Space Administration and the National Science Foundation.

REFERENCES

Anderson L. D., Bania T. M., Balser D. S., Rood R. T., 2011, ApJS, 194, 32
Beltran M. T., Cesaroni R., Neri R., Codella C., 2011, A&A, 525, 151
Benjamin R. A., Churchwell E., Babler B. L., 2003, PASP, 115, 953
Bernasconi P. A., Maeder A., 1996, A&A, 307, 829
Beuther H., Linz H., Henning Th., 2011, A&A, 531, 26
Carey S. J., Clark F. O., Egan M. P., Price S. D., Shipman R. F., Kuchar T. A., 1998, ApJ, 508, 721
Carey S. J., Feldman P. A., Redman R. O., Egan M. P., MacLeod J. M., Price S. D., 2000, ApJ, 543, L157
Caswell J. L., Murray J. D., Roger R. S., Cole D. J., Cooke D. J., 1975, A&A, 45, 239
Chen X., Shen Z., Li J., Xu Y., He J., 2010, ApJ, 710, 150
Churchwell E. et al., 2009, PASP, 121, 213
Clemens D. P., Sanders D. B., Scoville N. Z., Solomon P. M., 1986, ApJS, 60, 297
Corbel S., Eikenberry S. S., 2004, A&A, 419, 191
Cyganowski C. J. et al., 2008, AJ, 136, 2391
Dame T. M., Thaddeus P., 2008, ApJ, 683, 143
Downes D., Wilson T. L., Beiging J., Wink J., 1980, A&AS, 40, 379
Ellingsen S. P., 2006, ApJ, 638, 241
Fazio G. G., Hora J. L., Allen L. E., 2004, ApJS, 154, 10
Flaherty K. M., Pipher J. L., Megeath S. T., Winston E. M., Gutermuth R. A., Muzerolle J., Allen L. E., Fazio G. G., 2007, ApJ, 663, 1069
Furness J. P., Crowther P. A., Morris P. W., Barbosa C. L., Blum R. D., Conti P. S., van Dyk S. D., 2010, MNRAS, 403, 1433
Gerin M. et al., 2010, A&A, 521, L16
Goldsmith P. F., Mao X. J., 1983, ApJ, 265, 791
Gomez L., Wyrowski F., Pillai T., Leurini S., Menten K. M., 2011, A&A, 529, A161
Goss W. M., Matthews H. E., Winnberg A., 1978, A&A, 65, 307
Grave J. M. C., Kumar M. S. N., 2009, A&A, 498, 147
Green J. A., McClure-Griffiths N. M., Caswell J. L., Ellingsen S. P., Fuller G. A., Quinn L., Voronkov M. A., 2009, ApJ, 696, L156
Green J. A. et al., 2010, MNRAS, 409, 913
Gutermuth R. A., Myers P. C., Megeath S. T., 2008, ApJ, 674, 336
Gutermuth R. A., Megeath S. T., Myers P. C., Allen L. E., Pipher J. L., Fazio, G. G., 2009, ApJS, 184, 18
Haschick A. D., Ho, P. T. P., 1983, ApJ, 267, 638
Henning T., Linz H., Krause O., Ragan S., Beuther H., Launhardt R., Nielbock M., Vasyunina T., 2010, 518, L95
Jackson J. M., Chambers E. T., Rathborne J. M., Simon R., Zhang Q., 2008, in Beuther H., Linz H., Henning T., eds, ASP Conf. Ser. Vol. 387, Massive Star Formation: Observations Confront Theory. Astron. Soc. Pac., San Fransisco, p. 44
Johnstone D., Fiege J. D., Redman R. O., Feldman P. A., Carey S. J., 2003, ApJ, 588, 37
Kim K.-T., Koo B.-C., 2002, ApJ, 575, 327
Klaassen P. D., Wilson C. D., Keto E. R., Zhang Q., Galvan-Madrid R., Liu H. Y. B., 2011, A&A, 530, A53
Kryukova E., Megeath S. T., Gutermuth R. A., Pipher J., Allen T. S., Allen L. E., Myers P. C., Muzerolle J., 2012, AJ, 144, 31
Kurucz R., 1993, ATLAS9 Stellar Atmosphere Programs and 2 km/s grid. Kurucz CD-ROM No. 13, Smithsonian Astrophysical Observatory, Cambridge
Lada C. J. et al., 2006, AJ, 131, 1574
Liu H. B., Zhang Q., Ho, P. T. P., 2011, ApJ, 729, 100

Messineo M., Davies B., Figer D. F., Kudritzki R. P., Valenti E., Trombley C., Najarro F., Rich R. M., 2011, ApJ, 733, 41
Myers P. C., 2009, ApJ, 700, 1609
Neufeld D. A. et al., 2010, A&A, 518, L108
Olmi L., Cesaroni R., Walmsley C. M., 1996, A&A, 307, 5990
Pascucci I., Apai D., Henning T., Stecklum B., Brandl B., 2004, A&A, 426, 523
Peretto N., Fuller G. A., 2009, A&A, 505, 405
Persson C. M. et al., 2012, A&A, 543, A145
Pillai T., Wyrowski F., Menten K. M., Krgel E., 2006, A&A, 447, 929
Povich M. S., Whitney B. A., 2010, ApJ, 714, 285
Purcell C. R. et al., 2013, ApJS, 205, 1
Rathborne J. M., Jackson J. M., Chambers E. T., Simon R., Shipman R., Frieswijk W., 2005, ApJ, 630, L181
Rathborne J. M., Jackson J. M., Simon R., 2006, ApJ, 641, 389
Rathborne J. M., Simon R., Jackson J. M., 2007, ApJ, 662, 1082
Robitaille T. P., Whitney B. A., Indebetouw R., Wood K., 2007, ApJS, 169, 328
Rolffs R., Schilke P., Zhang Q., Zapata L., 2011, A&A, 536, 33
Rougoor G. W., Oort J. H., 1960, Proc. Natl. Acad. Sci. USA, 46, 1
Sanders D. B., Clemens D. P., Scoville N. Z., Solomon P. M., 1986, ApJS, 60, 1
Siess L., Dufour E., Forestini M., 2000, A&A, 358, 593
Simon R., Rathborne J. M., Shah R. Y., Jackson J. M., Chambers E. T., 2006, ApJ, 653, 1325
Smith N. et al., 2010, 406, 952
Soifer B. T., Puetter R. C., Russell R. W., Willner S. P., Harvey P. M., Gillett F. C., 1979, AJ, 232, L53
Sollins P. K., Zhang Q., Keto E., Ho, P. T. P., 2005, ApJ, 624, L49
Stern D. et al., 2005, ApJ, 631, 163
Stier M. T., Fazio G. G., Roberge W. G., Thum C., Wilson T. L., Jaffe D. T., 1982, ApJS, 48, 127
Tackenberg J. et al., 2012, A&A, 540, A113
Werner M. W. et al., 2004, ApJS, 154, 1
Whitney B. A. et al., 2008, AJ, 136, 18
Wilson T. L., 1974, A&A, 31, 83

This paper has been typeset from a TEX/LATEX file prepared by the author.